

Design, Engineering and Optimization of a Grid-Tie Multicell Inverter for Energy Storage Applications

A. Ashraf Gandomi¹, S. Saeidabadi¹, M. Sabahi¹, M. Babazadeh¹, and Y. Ashraf Gandomi²

¹Department of Electrical and Computer Engineering,
University of Tabriz, Tabriz

²Electrochemical Energy Storage and Conversion Laboratory,
Department of Mechanical, Aerospace and Biomedical Engineering,
University of Tennessee, Knoxville, Tennessee, USA

Multilevel converters have found many applications within renewable energy systems thanks to their unique capability of generating multiple voltage levels. However, these converters need multiple DC sources and the voltage balancing over capacitors for these systems is cumbersome. In this work, a new grid-tie multicell inverter with high level of safety has been designed, engineered and optimized for integrating energy storage devices to the electric grid. The multilevel converter proposed in this work is capable of maintaining the flying capacitors voltage in the desired value. The solar cells are the primary energy sources for proposed inverter where the maximum power density is obtained. Finally, the performance of the inverter and its control method simulated using PSCAD/EMTDC software package and good agreement achieved with experimental data.

Index Terms—Multicell inverter; Grid-tie multilevel inverter; Maximum Power Point Tracking; Flying capacitor; Energy storage devices.

I. INTRODUCTION

THE application of renewable energy sources (i.e. solar wind energy) into an electric grid requires high performance energy storage devices along with various types of power electronics (i.e. rectifiers, converters and inverters). Figure 1 includes the schematic of a hybrid energy storage system in which a renewable energy source (here photovoltaic modules) along with an energy storage device has been implemented to the electric grid via the utilization the multilevel inverters [1], [2], [3].

As shown in Fig. 1, battery-based devices and hydrogen-based energy storage technologies are promising. A good review on the battery- and hydrogen-based energy storage has been provided recently [4]. For hydrogen based energy storage, an electrolyzer along with a polymer electrolyte membrane (PEM) fuel cells are utilized. Although being very promising, the water management for electrolyzers and PEM fuel cells remains a challenging issue to be addressed [5], [6]. Also, the hydrogen gas storage technologies and infrastructure for regenerative hydrogen fuel cell systems is required to be addressed appropriately [7], [8]. Several battery technologies are developed for energy storage technologies that redox flow batteries are among the most promising devices. However engineering the redox flow batteries for optimum operation requires detailed mathematical models [9], [10], [11] and experimental diagnostics [12], [13].

The application of multilevel converters for the renewable energy systems has been increased recently [14], [15], [16], [17]. This is mostly because of high energy output (in the range of MW), high efficiency and low electromagnetic interference being offered via their application [18], [19], [20].

Manuscript submitted August 26, 2017. Corresponding author: A. Ashraf Gandomi (email: a.ashrafgandomi91@ms.tabrizu.ac.ir).

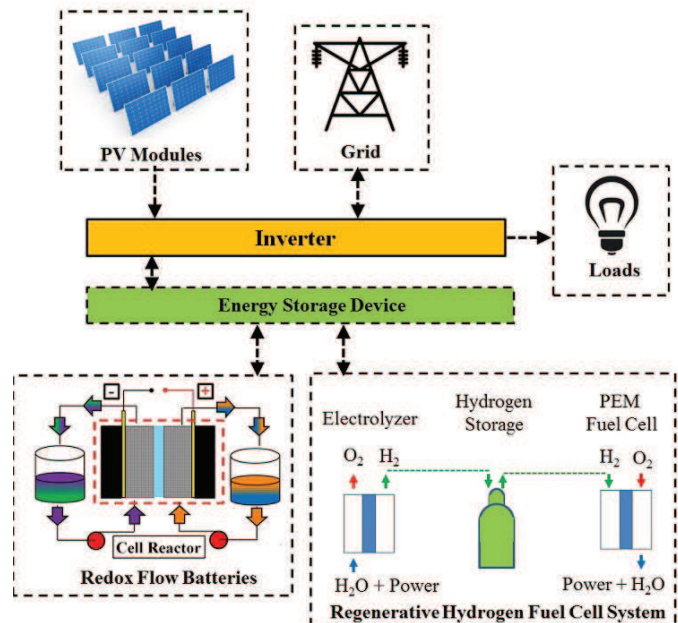


Fig. 1: Schematic of a hybrid energy system.

Three-level converter first proposed by Nabae [21] and the converters with increased number of levels developed later to obtain higher levels of voltage and reduce the harmonic content of the output voltage. However, increasing the number of voltage levels results in increased system complexity and severe voltage balancing problems. Different topologies for these types of converters have been utilized including Neutral Point Clamped (NPC) and variant types of multicell inverters [22], [23], [24]. The NPC topology suffers from diode clamped and capacitor voltage balancing issues where the multicell

TABLE I: Comparison of different inverters components

Type	# DC Sources	Magnitude	# Switches	# Capacitors
CM	n	E/n	$4n$	0
FCM	2	E	$4n$	$2n - 1$
SM	2	E	$4n$	$2(n - 1)$
DFCM	1	E	$2n + 2$	$n - 1$

inverters do not suffer from the same issue. Therefore, multicell inverters are promising candidates to generate increased voltage levels for high power generation applications. The multicell inverters have different types including the Cascaded Multicell (CM), Flying Capacitor Multicell (FCM) and Stacked Multicell (SM) inverters [25], [26], [27]. The FCM inverters along with the SM inverters have many unique advantages for medium voltage applications such as operation without transformer and naturally capacitor voltage balancing ability. A comparison of the different components being used with these different inverters for generating levels had been provided in Table. I.

Table. I. comparison of different inverters components

The advantages of DFCM compared to conventional structures are eliminating the common point of DC sources, reducing the number of input DC sources, switches and capacitors. However, this structure is an island and in the grid-tie form of this inverter with presented control method, some difficulties arise including the power transfer from grid to input source and the possibility of discharging flying capacitors in case of connecting to the Photovoltaic (PV) cells. In this paper a new topology for grid-tie multicell inverter has been developed. The proposed inverter has been designed based upon the DFCM inverter and accordingly shares the common advantages associated with the DFCMs including the elimination of common point of DC source, reduced number of DC sources and increased number of voltage levels. Also, the new design assures higher level of safety and via its utilization, the common problems related to the DFCMs has been eliminated (while extracting the maximum power from PV cells).

II. PROPOSED MULTILEVEL INVERTER

The proposed inverter is shown in Fig. 2. In this structure independent of the number of inverter cells and generated voltage levels, only the switches S_n and P_n in $cell_n$ are bidirectional. The oscillations of the PV cells voltage is mostly caused by climatic oscillations. In case of low PV cells and because of the cascaded diode of PV cells would not be functional and therefore, the possibility of discharging flying capacitors or grid voltage on the PV cells increases. Discharging the grid in the positive half cycle, the negative half cycle and discharging the flying capacitors are shown in Fig. 3. According to Fig. 3, in the proposed inverter, by using only two bidirectional switches, there would be no chance of discharging the grid and the flying capacitors on the PV cells.

Table II, includes the switching states within the proposed inverter for generating 5-level output voltage. In this table, when the switch is on, the corresponding state number is one and for the off position it is zero. Also X in this table due to

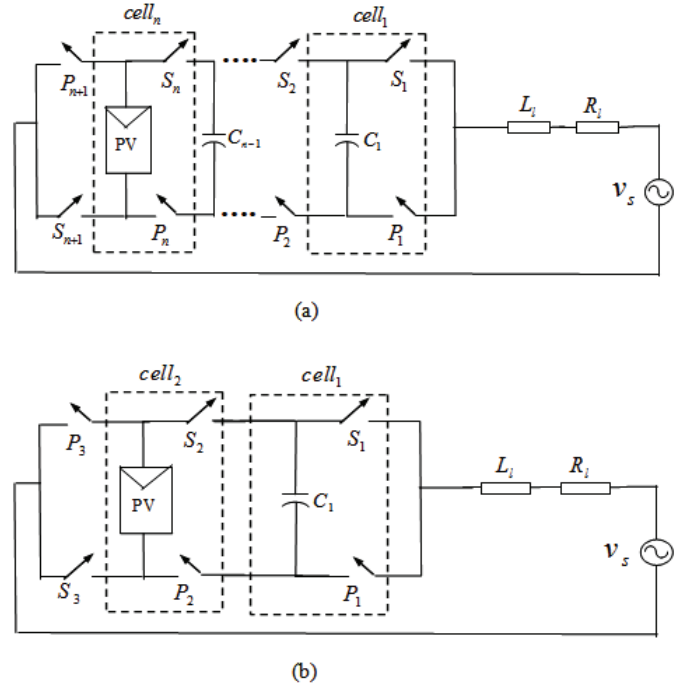


Fig. 2: (a) Proposed grid-tie multicell inverter and (b) Proposed 5-level grid-tie multicell inverter.

TABLE II: Switching states in the proposed inverter

States	S_1	S_2	S_3	P_1	P_2	P_3
1	1	1	1	0	X	0
2	1	0	1	0	1	0
3	1	1	0	0	X	1
4	0	1	0	1	0	1
5	0	X	0	1	1	1

modes of charging or discharging of flying capacitor C_1 , is either one or zero. Based on this table, in the states 2 and 4, charging or discharging of C_1 happens naturally, while in the other states, due to value of X, C_1 can be charged. The voltage balancing algorithm of C_1 in positive half cycle is shown in Fig. 3. Based on this figure, if the measured value of voltage of capacitor C_1 is lower than its set value (v_{C1}), P_2 (or S_2) will be on in the state 1 (or 3). This can continue until the voltage of C_1 reaches its specified value then P_2 will be off.

III. PROPOSED CONTROL METHOD

In the control method, it is assumed that the inverter output current tracks the favorite sinusoidal reference current. Also as it is shown in Fig. 5, it is assumed that the proposed inverter (base on IEEE 1547 standard) does not exchange any reactive power with the grid and only active power exchanges, therefore:

$$v_s(t) = V_m \sin(\omega t) \quad (1)$$

$$i_r(t) = I_m \cdot \sin(\omega t) \quad (2)$$

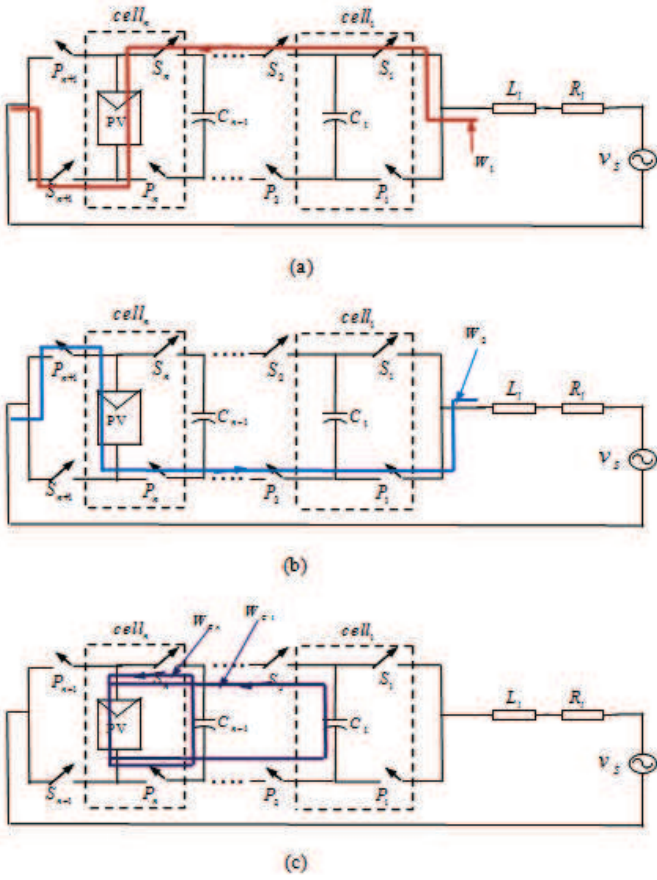


Fig. 3: (a) Discharging the grid in the positive half cycle, (b) Discharging the grid in the negative half cycle and (c) Discharging the flying capacitors.

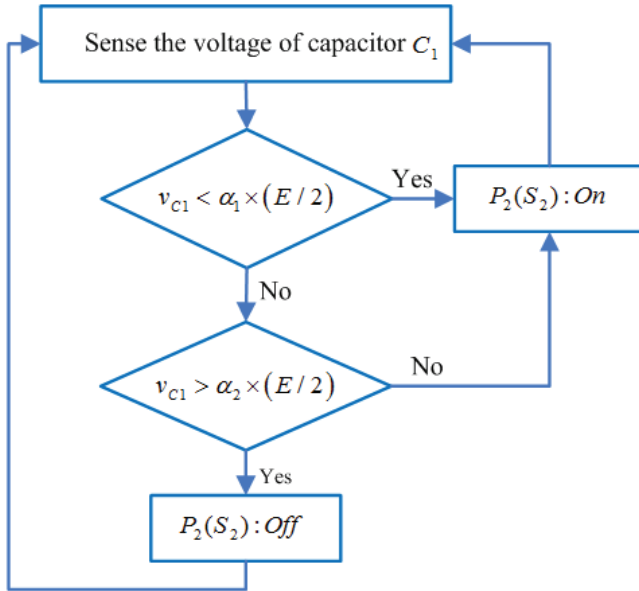


Fig. 4: Algorithm of charge and discharge of capacitor in the positive half cycle of output voltage.

Figure 6 shows five output voltage levels that have been considered for the proposed inverter. The proposed control

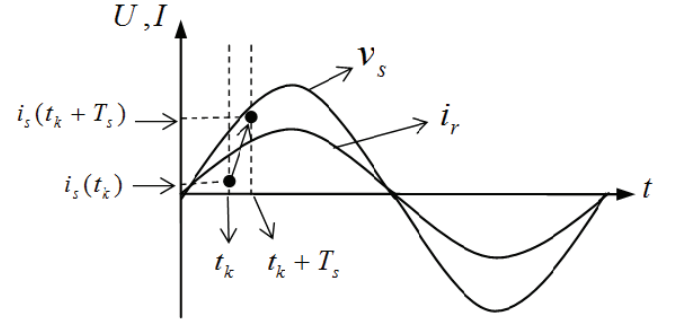


Fig. 5: Proposed control method.

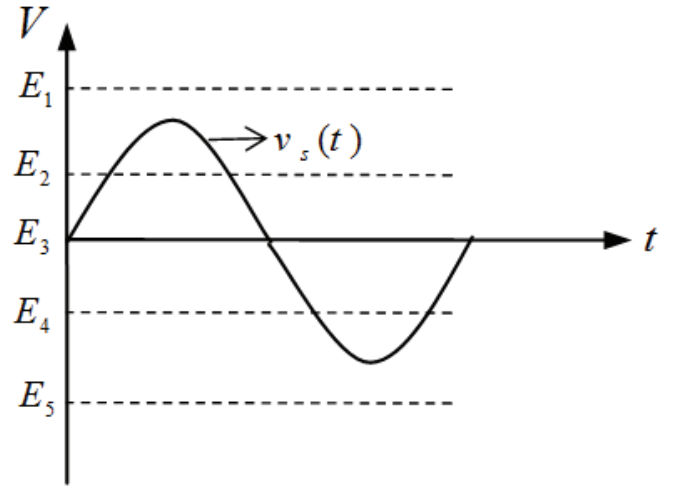


Fig. 6: The output voltage levels of proposed inverter.

method should be capable of injecting power from inverter to grid at different operating conditions and therefore, the maximum voltage generated through the inverter (E_1) should be greater than the grids maximum voltage (V_m).

Due to generating output voltage with low Total Harmonic Distortion (THD), the values of output voltages are considered as follows:

$$E_2 = \frac{E_1}{2}, E_3 = 0, E_4 = \frac{-E_1}{2}, E_5 = -E_1 \quad (3)$$

The grid voltage and reference current is calculated according to (4) and (5) assuming the circuit current in the constant t_k is $i_s(t_k)$:

$$v_s(t_k) = V_m \sin(\omega t_k) \quad (4)$$

$$i_r(t_k) = I_m \sin(\omega t_k) \quad (5)$$

The equivalent circuits of the proposed inverter are shown in Fig. 7.

In Fig. 7, R_l and L_l are the line resistance and inductance between inverter and grid and V_0 . According to Fig. 7(a):

$$L_l \frac{di_s(t)}{dt} + R_l i_s(t) = V_0 + v_s(t) = V_0 + V_m \sin(\omega t) \quad (6)$$

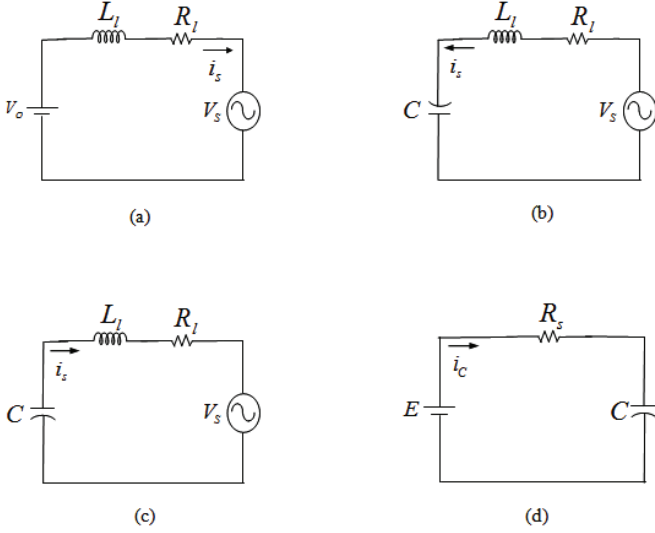


Fig. 7: (a) Equivalent circuit of the system, (b) Equivalent circuit of capacitor discharging state, (c) Equivalent circuit of capacitor discharging state and (d) Equivalent circuit of capacitor charging.

Then:

$$i_s(t_k) = I_k \quad (7)$$

$$i_s(t) = K_1 e^{-\frac{R_l t}{L_l}} + K_2 \sin(\omega t) + K_3 \cos(\omega t) + \frac{V_0}{R_l} \quad (8)$$

$$K_1 = \frac{I_k - \frac{V_m}{R_l^3 + L_l^2 \omega^2 R_l} + \frac{V_m L_l \omega}{R_l^2 + L_l^2 \omega^2}}{e^{-\frac{R_l t}{L_l}}} \quad (9)$$

$$K_2 = \frac{V_m}{R_l^3 + L_l^2 \omega^2 R_l} \quad (10)$$

$$K_3 = \frac{-V_m L_l \omega}{R_l^2 + L_l^2 \omega^2} \quad (11)$$

In constant t_k , $i_s(t_k)$ is measured. Control system using (8), calculates five current for a five-level output voltage of inverter during the next switching period. Therefore, for five output voltage levels, five cost functions can be written as follow:

$$\Delta I = |i_r t_k + T_s - i_s(t_k + T_s)| \quad (12)$$

From (12), proper switching state and consequently proper output voltage can be applied. Initially, when the inverter connects to the network, the initial voltage of the capacitor is zero. At this point, no impulse current is drawn until the capacitor voltage reaches the proper value where the grid current is bypassed by S_1 , S_2 and P_3 and simultaneously input source charged the capacitor by S_2 and P_2 . When the capacitor voltage reaches its proper value, control method will follow their normal operation. In Fig. 8(a) and (b), upper waveforms are inverter output voltage and the lower waveforms are the

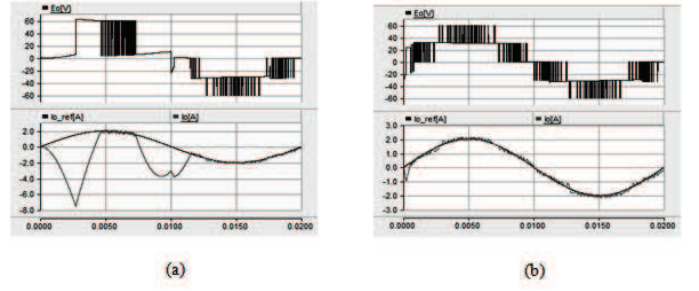


Fig. 8: Voltage stability (a) without initial control method and (b) with initial control method.

inverter output current. Based on Fig. 8(a), if the initial control method does not apply, 60% of the original period (0.012 seconds) would be required for inverter to reach its own stable performance. This situation also results in over-drawn current as high as four times of the maximum nominal current through the circuit, which potentially damages the whole circuit. However, this situation has improved in Fig. 8(b) where the response time has decreased to about 0.0005 seconds. Therefore, the inverter only requires approximately 2.5% of the original period to reach its own stable performance. Also in this case, the drawn current is within the safe range.

IV. FLYING CAPACITOR VOLTAGE BALANCING METHOD

In this section, the method of capacitor voltage balancing is investigated. Based on Table II, the capacitor is discharged in the duration that output voltage equals to $E/2$ with positive current of circuit and output voltage equal to $-E/2$ with negative current of circuit. Based on the equivalent circuit of capacitor discharging states (Fig. 7(b) and (c)):

$$v_s(t) = V_m \sin(\omega t) \quad (13)$$

$$i_s(t) = I_m \sin(\omega t) \quad (14)$$

$$v_s(t) = V_c(t) + L_l \frac{di_L(t)}{dt} + R_l i_s(t) \quad (15)$$

$$v_c(t) = \sqrt{(V_m - R_l I_m)^2 + (L_l I_m)^2} \sin[\omega t + \arcsin(\frac{-L_l I_m}{\sqrt{(V_m - R_l I_m)^2 + (L_l I_m)^2}})] \quad (16)$$

In the equations formulated earlier ((13) to (16)), is the grid voltage and $v_c(t)$ is the capacitor voltage. Also $i_s(t)$ is the circuit current that should be the sine wave because of tracking the reference sine wave. According to Table II, unlike the case of the capacitor discharging state that was possible only in two operating modes, charging of capacitor happens in all five operating modes. When the inverter output voltage is equal to $E/2$ with negative current of circuit and equal to $-E/2$ with positive current of circuit, capacitor is charged naturally. But in the duration that output voltage is equal to

E or zero, charging of capacitor is controlled by switch P_2 and within the range that output voltage is equal to $-E$ or zero, charging of capacitor is controlled by switch S_2 . The capacitor charging circuit in all five modes is shown in Fig. 7(d). In this figure, R_s is the resistance of switches per current loop, therefore the following equations for a capacitor charging state can be obtained:

$$E = R_s i_c(t) + v_c(t) \quad (17)$$

$$i_c(t) = c \frac{dv_c(t)}{dt} \quad (18)$$

$$v_c(t_1) = V_1 \quad (19)$$

$$v_c(t) = E + \frac{V_1 - E}{e^{\frac{-t}{R_s c}}} e^{\frac{-t_1}{R_s c}} \quad (20)$$

In the (17) and (18), $v_c(t)$ and $i_c(t)$ are the voltage and current of capacitor respectively. The value of R_s is very small, therefore the time of capacitor charging is short and capacitor is charged rapidly. However, capacitor discharging state is a swinging relation. Thus, capacitor voltage can be adjusted to the desired value just by controlling the charging state of capacitor voltage.

V. DETERMINATION OF CAPACITANCE OF FLYING CAPACITOR

The capacitor charging and discharging states is shown in Fig. 7(b)-(d). The value of R_s is very small, therefore the time of capacitor charging is short and capacitors capacitance determination is applied only for discharging state of capacitor.

$$i_c = c \frac{\Delta V_c}{\Delta t} \quad (21)$$

Here, Δt is the time of single switching duty cycle. ΔV_c is the capacitor rated voltage drop in one switching duty cycle which is assumed five percent of capacitor rated voltage. Consequently:

$$T_s = \Delta t \quad (22)$$

$$\Delta v_c = 0.05 \frac{E}{2} \quad (23)$$

Circuit current in Fig. 7, (i_s), is the sine wave that can be formulated as follow:

$$i_s = i_m \sin(\omega t) \quad (24)$$

i_c in (21) is equal to maximum value of current in (24), I_m , and therefore (25) is utilized to calculate the capacitors capacitance.

$$c = \frac{i_c \Delta t}{\Delta v_c} \quad (25)$$

VI. MPPT IN THE PROPOSED INVERTER

Maximum power of PV cells in any constant is shown by P_{PV} . The efficiency of the system is η , the output is P_{ac} . Therefore:

$$P_{ac} = \eta P_{pv} \quad (26)$$

And:

$$P_{ac} = V_s I_s \quad (27)$$

Here, V_s and I_s are the RMS value of grid voltage and current respectively. Therefore, if one assigns any values for P_{PV} and V_s , the appropriate value for I_{ref} capable of tracking I_s determined and this guarantees the maximum output power from solar cells.

VII. VOLTAGE LOSS CALCULATION

In this section, the loss calculation has been done for the proposed topology. The loss calculation contains switches losses and capacitor losses.

A. Switches losses

Mainly conduction and switching losses are calculated for switches. Every power switch contains a transistor (MOSFET) and a diode, and therefore, the instantaneous conduction loss of these elements is calculated using (28) and (29), respectively [21]:

$$P_{c,T}(t) = [R_T i(t)] i(t) \quad (28)$$

$$P_{c,D}(t) = [V_D + R_D i(t)] i(t) \quad (29)$$

Where V_D is considered as forward voltage drop of the diode. R_T and R_D are equivalent resistance of the transistor and diode. At any time $N_T(t)$ transistor and $N_D(t)$ diodes are in current path, so the average conduction power losses can be written as:

$$P_C = \frac{1}{2\pi} \int_0^{2\pi} [N_T(t) P_{c,T}(t) + N_D(t) P_{c,D}(t)] dt \quad (30)$$

The switching losses occur during turn on and turn off period of switches. For simplicity, the linear approximation of voltage and current of switches during the switching period is considered. Based on this assumption, the switching loss is calculated as follows:

$$E_{off,J} = \int_0^{t_{off}} (v(t) i(t)) dt = \int_0^{t_{off}} \left[\left(\frac{V_{sw,J} t}{t_{off}} \right) \left(-\frac{I''(t - t_{off})}{t_{off}} \right) \right] dt = \frac{1}{6} V_{sw,J} I'' t_{off} \quad (31)$$

$$E_{on,J} = \int_0^{t_{on}} (v(t) i(t)) dt = \int_0^{t_{on}} \left[\left(\frac{V_{sw,J} t}{t_{on}} \right) \left(-\frac{I'(t - t_{on})}{t_{on}} \right) \right] dt = \frac{1}{6} V_{sw,J} I' t_{on} \quad (32)$$

$E_{off,J}$ and $E_{on,J}$ are turn off and turn on loss of the switch J , I is the current through the switch before turning off, I is the current through the switches after turning on and $V_{sw,J}$ is the off-state voltage on the switch. The switching power loss is equal to the sum of all turns off and turns on energy losses in the fundamental frequency of the output voltage; as a result, average switching power loss can be calculated as follow:

$$P_{sw} = f \sum_{J=1}^{N_{switch}} \left(\sum_{k=1}^{N_{on,J}} E_{on,Jk} + \sum_{k=1}^{N_{off,J}} E_{off,Jk} \right) \quad (33)$$

f is the fundamental frequency, $N_{on,J}$ and $N_{off,J}$ are the number of turning on and off the J^{th} switch during fundamental frequency. $E_{on,Jk}$ is the energy loss of the J^{th} switch during the k^{th} turning on and $E_{off,Jk}$ is the energy loss of the J^{th} switch during the k^{th} turning off.

B. Capacitor losses

The capacitor losses consist of capacitor voltage ripple losses P_{rip} and conduction losses P_{cond} . The voltage ripple of capacitor is calculated as follow:

$$\Delta V_{rip} = \frac{1}{C} \int_{t_-}^{t_+} i_C dt \quad (34)$$

Where i_C , the transient current of the capacitor, equals to the line current. t_- to t_+ is the interval that the capacitor is connected in series with DC voltage sources. So, voltage ripple loss is written as follow:

$$P_{rip} = C \Delta V_{rip}^2 f \quad (35)$$

f is the frequency of the output voltage. The conduction losses can be written as follow:

$$P_{cond} = 2f \int_{t_-}^{t_+} r_C i_C^2 dt \quad (36)$$

Where r_C is the internal resistance of the capacitor. Total loss of the proposed topology is equal:

$$P_{loss} = P_C + P_{sw} + P_{rip} + P_{cond} \quad (37)$$

Finally, the efficiency of converter is written as follow:

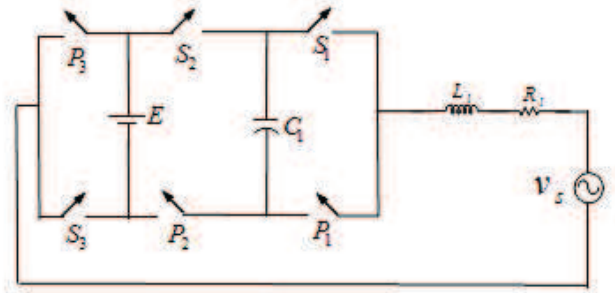
$$\eta = \frac{P_{out}}{P_{in}} = \frac{P_{in} - P_{loss}}{P_{in}} \quad (38)$$

Where P_{out} and P_{in} are output power and input power of converter.

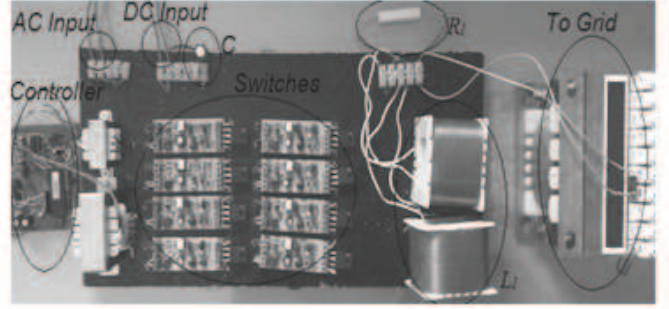
VIII. SIMULATION RESULTS AND EXPERIMENTAL VERIFICATION

The simulation has been done by PSCAD / EMTDC. The circuit used in the simulation and the experimental set up and the value of elements used in both of them are shown in Fig. 9 and Table III. Due to the limitation of laboratory components, DC voltage source is used instead of PV cells.

For further analysis of inverters performance, input DC voltage source is changing from 60 V to 65 V in 0.04 s



(a)



(b)

Fig. 9: (a) Circuit of simulation of 5-level proposed inverter and (b) Picture of experimental set up.

TABLE III: Quantitative values used for simulation

Parameter	Value	Attribute
E	60	Inverter Input Voltage
V_m	48	Grid maximum voltage
R_l	0.1	Line Resistance
L_l	0.005	Line Inductance
C_1	500	Flying Capacitor
f_s	10	Switching Frequency
f_g	50	Grid Frequency
$R_{D-S,on}$	0.4	Transistor Drain-Source On-State Resistance

and from 65V to 55 V in 0.06 s, the results are shown in Fig. 10. According to Fig. 10, the proposed inverter with proposed control method produces 5-level voltage and tracks the reference current properly in the variation of DC source. Also, Flying capacitors voltage is balanced in its specified value (half of the input DC source).

In the experimental circuit, inverter output voltage and current for 5-level output voltage is shown in Fig. 11. This figure indicates that the proposed inverter produces an output voltage waveform with 5 levels with maximum output level of 60 V. Also in this inverter, output current of approximately 2 A tracks the reference current properly that is in phase with grid voltage, therefore the proposed inverter can exchange active power with the grid. In the laboratory condition the measured output and input power are about 48 (W) and 52.8 (W), respectively. Therefore, the efficiency is equal 90.91%. Based on the efficiency calculation, it is about 91.13%. Accordingly, the computed efficiency has good accordance with

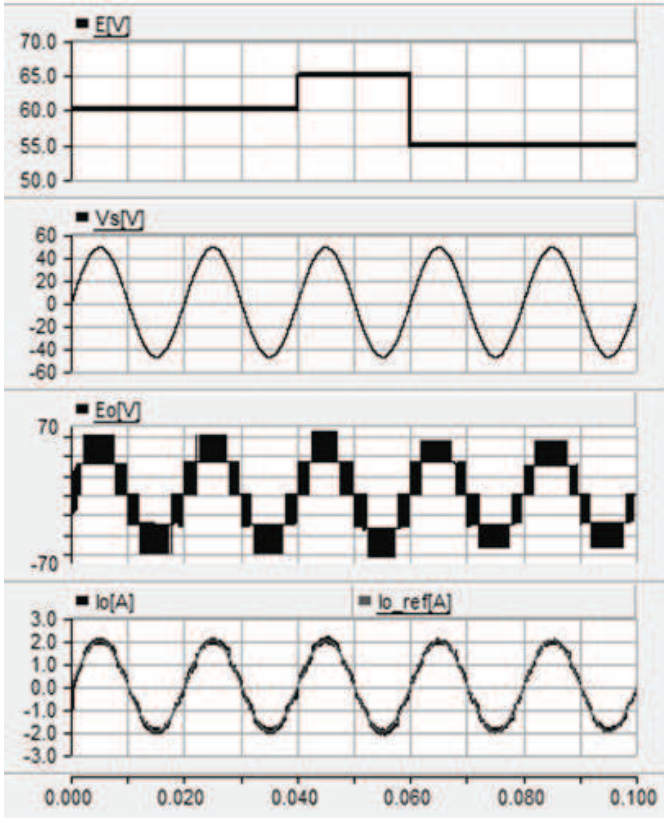


Fig. 10: Input DC source (E), grid voltage (V_s), inverter output voltage (E_o) and inverter output current (I_o).

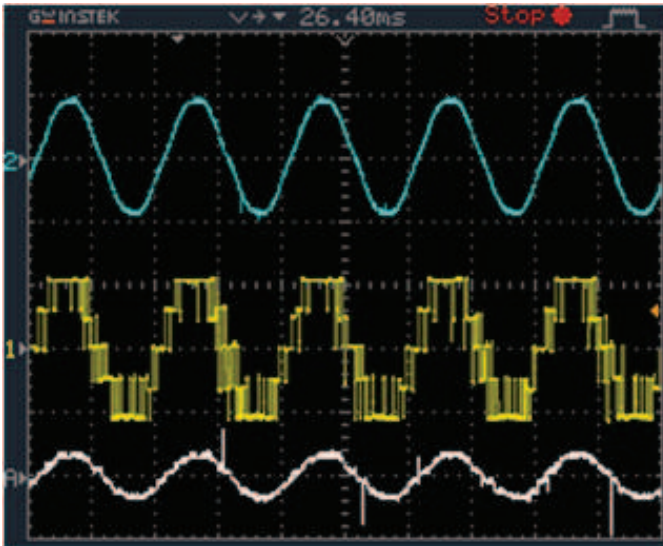


Fig. 11: Grid voltage (50V/div), inverter output voltage (50V/div) and current (4A/div), 10ms/div.

the measured efficiency. Voltage and voltage ripples of flying capacitor are shown in Fig. 12. Base on Fig. 12, the voltage of flying capacitor is balanced on the desired value with 0.2 ripples.

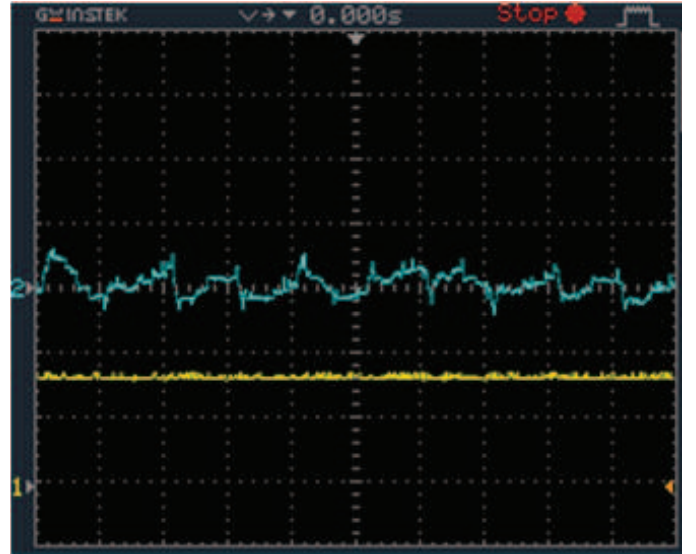


Fig. 12: Voltage ripples (200mV/div) and voltage of flying capacitor (20V/div), 5ms/div.

TABLE IV: Abbreviations

DC	Direct Current
MPPT	Maximum Power Point Tracking
NPC	Neutral Point Clamped
CM	Cascaded Multicell
FCM	Flying Capacitor Multicell
SM	Stacked Multicell
DFCM	Double Flying Capacitor Multicell
PV	Photovoltaic
THD	Total Harmonic Distortion
MOSFET	MetalOxideSemiconductor Field-Effect Transistor

IX. CONCLUSION

In the proposed inverter compared to the structure of DFCM, independent of the inverter cell number and the number of generated voltage levels, by replacing only two unidirectional switches with two bidirectional switches, network connectivity with high safety is provided. Also, this inverter with proposed control method has unique abilities such as capacitor voltage balancing in any desired value and obtaining maximum power from PV cells. Theoretically there is no limitation for the number of flying capacitors for balancing the voltage. The proposed control method tracks maximum power point of PV cells through assuring the equal magnitude for the input and output power. Through this unique controlling methodology, the MPPT is performed just by the inverter itself. Finally, the mathematical analysis and simulation results are used to verify the operation of proposed inverter and control method. The design, engineering and optimization procedure explained in this work provides further insight for designing multilevel inverters to be used in hybrid systems equipped with various energy storage devices (i.e. redox flow batteries and regenerative hydrogen fuel cell systems).

TABLE V: Symbols

n	Number of cells
E	Magnitude of DC voltage source
v_s	Grid voltage
i_r	Reference current
V_m	Grid maximum voltage
i_s	Grid current
ω	Angular frequency of grid voltage
R_s	Resistance of switches per current path loop
$N_T(t)$	Number of Transistor in current path at any time
$N_D(t)$	Number of Diode in current path at any time
r_C	Internal resistance of capacitor
f_g	Grid frequency
f_s	Switching frequency

REFERENCES

- [1] A. A. Gandomi, K. Varesi, and S. H. Hosseini, "Dc-ac buck and buck-boost inverters for renewable energy applications," in *Power Electronics, Drives Systems & Technologies Conference (PEDSTC), 2015 6th*. IEEE, 2015, pp. 77–82.
- [2] S. Saeidabadi, A. A. Gandomi, and S. H. Hosseini, "A novel transformer-less photovoltaic grid-connected current source inverter with ground leakage current elimination," in *Power Electronics, Drive Systems & Technologies Conference (PEDSTC), 2017 8th*. IEEE, 2017, pp. 61–66.
- [3] A. A. Gandomi, S. Saeidabadi, and M. Sabahi, "Maximum power point tracking control method in high gain transformer-based inverters for photovoltaic application," in *Power Electronics, Drive Systems & Technologies Conference (PEDSTC), 2017 8th*. IEEE, 2017, pp. 137–142.
- [4] M. A. Pellow, C. J. Emmott, C. J. Barnhart, and S. M. Benson, "Hydrogen or batteries for grid storage? a net energy analysis," *Energy & Environmental Science*, vol. 8, no. 7, pp. 1938–1952, 2015.
- [5] Y. A. Gandomi and M. M. Mench, "Assessing the limits of water management using asymmetric micro-porous layer configurations," *ECS Transactions*, vol. 58, no. 1, pp. 1375–1382, 2013.
- [6] Y. A. Gandomi, M. Edmundson, F. Busby, and M. M. Mench, "Water management in polymer electrolyte fuel cells through asymmetric thermal and mass transport engineering of the micro-porous layers," *Journal of The Electrochemical Society*, vol. 163, no. 8, pp. F933–F944, 2016.
- [7] M. Zehsaz, F. V. Tahami, and Y. A. Gandomi, "The plastic work curvature criterion in evaluating gross plastic deformation for pressure vessels with conical heads," in *Applied Mechanics and Materials*, vol. 50. Trans Tech Publ, 2011, pp. 93–99.
- [8] M. Zehsaz, F. V. Tahami, and Y. A. Gandomi, "Bifurcation buckling of pressurized conical vessels," *International Journal of Advances in Engineering & Technology*, vol. 3, no. 2, p. 108, 2012.
- [9] Y. A. Gandomi, T. A. Zawodzinski, and M. M. Mench, "Concentrated solution model of transport in all vanadium redox flow battery membrane separator," *ECS Transactions*, vol. 61, no. 13, pp. 23–32, 2014.
- [10] A. Yousefzadi Nobakht and S. Shin, "Anisotropic control of thermal transport in graphene/si heterostructures," *Journal of Applied Physics*, vol. 120, no. 22, p. 225111, 2016.
- [11] Y. A. Gandomi, D. Aaron, T. Zawodzinski, and M. Mench, "In situ potential distribution measurement and validated model for all-vanadium redox flow battery," *Journal of The Electrochemical Society*, vol. 163, no. 1, pp. A5188–A5201, 2016.
- [12] Y. A. Gandomi, D. Aaron, and M. Mench, "Coupled membrane transport parameters for ionic species in all-vanadium redox flow batteries," *Electrochimica Acta*, vol. 218, pp. 174–190, 2016.
- [13] Y. Ashraf Gandomi, D. S. Aaron, and M. M. Mench, "Influence of membrane equivalent weight and reinforcement on ionic species crossover in all-vanadium redox flow batteries," *Membranes*, vol. 7, no. 2, p. 29, 2017.
- [14] S. Saeidabadi, A. A. Gandomi, and M. Sabahi, "Two new transformer-based isolated seven-level inverters," in *Power Electronics, Drive Systems & Technologies Conference (PEDSTC), 2017 8th*. IEEE, 2017, pp. 195–200.
- [15] S. H. Hosseini, K. Varesi, J. F. Ardashir, A. A. Gandomi, and S. Saeidabadi, "An attempt to improve output voltage quality of developed multi-level inverter topology by increasing the number of levels," in *Electrical and Electronics Engineering (ELECO), 2015 9th International Conference on*. IEEE, 2015, pp. 665–669.
- [16] A. A. Gandomi, K. Varesi, and S. H. Hosseini, "Control strategy applied on double flying capacitor multi-cell inverter for increasing number of generated voltage levels," *IET Power Electronics*, vol. 8, no. 6, pp. 887–897, 2015.
- [17] A. A. Gandomi, S. Saeidabadi, S. H. Hosseini, E. Babaei, and M. Sabahi, "Transformer-based inverter with reduced number of switches for renewable energy applications," *IET Power Electronics*, vol. 8, no. 10, pp. 1875–1884, 2015.
- [18] K. Varesi, A. A. Gandomi, S. Hosseini, M. Sabahi, and E. Babaei, "An improved structure for multi-input high step-up dc-dc converters," in *Power Electronics, Drive Systems & Technologies Conference (PEDSTC), 2017 8th*. IEEE, 2017, pp. 241–246.
- [19] A. A. Gandomi, S. Saeidabadi, and S. H. Hosseini, "A high step up flying capacitor inverter with the voltage balancing control method," in *Power Electronics, Drive Systems & Technologies Conference (PEDSTC), 2017 8th*. IEEE, 2017, pp. 55–60.
- [20] S. Saeidabadi, A. A. Gandomi, S. H. Hosseini, M. Sabahi, and Y. A. Gandomi, "New improved three-phase hybrid multilevel inverter with reduced number of components," *IET Power Electronics*, 2017.
- [21] A. Nabae, I. Takahashi, and H. Akagi, "A new neutral-point-clamped pwm inverter," *IEEE Transactions on industry applications*, no. 5, pp. 518–523, 1981.
- [22] A. K. Sadigh, V. Dargahi, M. Abarzadeh, and S. Dargahi, "Reduced dc voltage source flying capacitor multicell multilevel inverter: analysis and implementation," *IET Power Electronics*, vol. 7, no. 2, pp. 439–450, 2013.
- [23] J. Rodríguez, S. Bernet, P. K. Steimer, and I. E. Lizama, "A survey on neutral-point-clamped inverters," *IEEE transactions on Industrial Electronics*, vol. 57, no. 7, pp. 2219–2230, 2010.
- [24] M. R. Banaei, M. R. J. Oskuee, and F. M. Kazemi, "Series h-bridge with stacked multicell inverter to quadruplicate voltage levels," *IET Power Electronics*, vol. 6, no. 5, pp. 878–884, 2013.
- [25] B. P. McGrath and D. G. Holmes, "Natural current balancing of multicell current source converters," in *Power Electronics Specialists Conference, 2007. PESC 2007. IEEE*. IEEE, 2007, pp. 968–974.
- [26] P. Lezana, R. Aguilera, and J. Rodríguez, "Fault detection on multicell converter based on output voltage frequency analysis," *IEEE Transactions on Industrial Electronics*, vol. 56, no. 6, pp. 2275–2283, 2009.
- [27] T. A. Meynard, M. Fadel, and N. Aouda, "Modeling of multilevel converters," *IEEE transactions on industrial electronics*, vol. 44, no. 3, pp. 356–364, 1997.